Analytica Chimica Acta 1029 (2018) 86–96

Contents lists available at ScienceDirect

Analytica Chimica Acta

journal homepage: www.elsevier.com/locate/aca

Surface enhanced Raman spectroscopy based immunosensor for ultrasensitive and selective detection of wild type p53 and mutant $p53_{R175H}$

Anna Rita Bizzarri*, Ilaria Moscetti, Salvatore Cannistraro

Biophysics & Nanoscience Centre, DEB, Università della Tuscia, Viterbo, Italy

HIGHLIGHTS

- Ultrasensitive detection of wild type p53 and of the p53R175H mutant down to attomolar.
- The immunosensor exhibited high selectivity and reproducibility.
- The developed approach is susceptible to be extended to the ultrasensitive detection of other biomarkers.

GRAPHICAL ABSTRACT

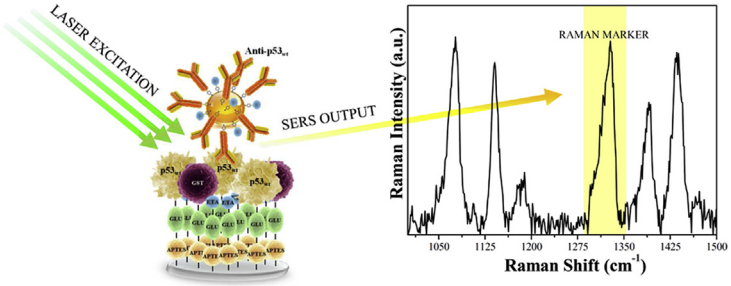

ARTICLE INFO

Article history:
Received 18 December 2017
Received in revised form
17 April 2018
Accepted 18 April 2018
Available online 21 April 2018

Keywords:
Surface enhanced Raman spectroscopy (SERS)
p53
Mutant $p53_{R175H}$
Ultrasensitive detection
Cancer biomarkers

ABSTRACT

p53 is a powerful transcription factor playing a pivotal role in the prevention of cancer development and in maintaining genome integrity. This oncosuppressor is found to be functionally inactivated by mutations in many human tumors. Accordingly, wild type p53 and its oncogenic mutants represent valuable cancer biomarkers for diagnostic and prognostic purposes. We developed a highly sensitive biosensor, based on Surface Enhanced Raman Spectroscopy, for detection of wild type p53 and of $p53_{R175H}$, which is one of the most frequent tumor-associated mutants of p53. Our approach combines the huge Raman signal enhancement, mainly arising from the plasmonic resonance effect on molecules close to gold nanoparticles, with the antigen-antibody biorecognition specificity. By following the enhanced signal of a specific Raman marker, intrinsic to the nanoparticle-antibody bioconjugation, we were able to push the antigen detection level down to the attomolar range in buffer and to the femtomolar range in spiked human serum. The method demonstrated a high reproducibility and a remarkable selectivity in discriminating between wild type p53 and $p53_{R175H}$ mutant, in both buffer and serum. A calibration plot was built and validated by ELISA for a reliable quantification of p53. These findings entitle our SERS-based immunosensor as a powerful and reliable tool for a non-invasive screening in human serum targeting p53 network. The approach could be easily extended to ultrasensitive detection of other markers of general interest, with feasible implementations into multiplex assays, functioning as lab-on-chip devices for several applications.

* Corresponding author. Biophysics & Nanoscience Centre, DEB, Università della Tuscia, Largo dell'Università, 01100, Viterbo, Italy.
E-mail address: bizzarri@unitus.it (A.R. Bizzarri).

https://doi.org/10.1016/j.aca.2018.04.049
0003-2670/

1. Introduction

p53 is a tumor suppressor protein playing an important role in cellular stress response by controlling pathways leading to cellular senescence, cell cycle arrest and apoptosis [1]. Unfortunately, in many tumors p53 is functionally inactivated by a strong down-regulation, with a consequent lowering of its current levels [2]. In addition, p53 is mutated in almost half of human cancers [3], and some oncogenic mutants are characterized by high stability and accumulation in the extracellular fluids of cancer patients [4–6]. Among these, $p53_{R175H}$ represents one of the most common p53 mutants found at progressively higher quantities in several tumors, such as lung, colon and rectal and with a particularly high incidence in breast tumor [7]. Therefore, wild type p53 ($p53_{wt}$) and the mutant $p53_{R175H}$ are valuable cancer biomarkers and their ultra-sensitive, non-invasive and selective detection is highly desired for early tumor diagnosis [8–10] and for evaluating invasiveness and prognosis [11], especially in connection with p53-based anticancer therapies [12]. In particular, the quantitative determination of p53 mutants at the very early stage, when therefore its concentration is very low, could be extremely relevant to diagnosis and also to therapy choice and optimization, also in the perspective of precision medicine applications [13].

Several sensitive analytical approaches were developed to detect p53 proteins, such as the enzyme-linked immunosorbent assay (ELISA) [10], electrochemical assays [14,15], Surface Plasmon Resonance sensing [16], Field-Effect Transistor biosensing [17], Surface Enhanced Raman Spectroscopy (SERS) [18,19] and others [20–22]. Ongoing efforts are currently focused on the improvement of sensitivity, selectivity, accuracy and specificity of the different sensing approaches aimed at detecting the p53-family proteins [23]. However, the intrinsically disordered character of this protein, concomitantly with its ability to target different partners within its network, makes such a task rather difficult [24,25].

Among other techniques, SERS, which is based on the huge enhancement of the Raman cross section when molecules are placed in close proximity of a nanostructured metal surface, able to exert electromagnetic, plasmonic and chemical effects [26], appears extremely promising [27–30].

In previous SERS works [18,31], we exploited the binding capacity of the protein Azurin for detecting p53 and its mutated isoforms. However, due to the extended binding regions recognized by Azurin, which involves both the N-terminal and the DNA binding domain of p53 proteins [32–34], we were not able to discriminate among $p53_{wt}$ and its mutated isoforms and, more importantly, we were not able to reach an ultra-low detection level, which could be important for early cancer diagnosis [35].

In the attempt to both achieve a reliable discrimination between wild type and mutated isoforms of p53 and reach a lower detection limit, we developed a method which combines the remarkable detection capability of the SERS technique with the unique biological specificity occurring between antigen-antibody pairs [36].

Two specific antibodies, able to target the antigens $p53_{wt}$ or its mutant $p53_{R175H}$, were bound to gold nanoparticles through a specific linker and by following a very reproducible chemical procedure, able to minimize non-specific interactions. We monitored then the enhanced Raman signal from a specific marker intrinsic to the nanoparticle-antibody bioconjugation. Accordingly, we were able to lower the detection level of both the $p53_{wt}$ and $p53_{R175H}$ antigens to a femtomolar concentration in human serum, and even down to the attomolar range in buffer. The achievement of such an unprecedented high sensitivity [15,31,37,38] took advantage of a careful tailoring and standardization of both the substrate and the detection probe functionalization chemistry, combined with immunosensing through appropriate antibodies able to maximize the capture process.

The detection method demonstrated a high reproducibility and a remarkable selectivity in discriminating between $p53_{wt}$ and $p53_{R175H}$ mutant, in both buffer and serum. Quantification of the antigen concentrations was validated by ELISA. All these features strongly highlight the potentiality of the proposed biosensing approach for early detection of cancers harbouring a strong down-regulation of $p53_{wt}$ and/or a tiny presence of the $p53_{R175H}$ mutant; providing concomitantly a remarkable tool to evaluate prognosis and efficacy of anticancer therapies. The method could be easily adapted for detection of other markers and it is even implementable as a lab-on-chip device for multiple applications.

2. Materials and methods

2.1. Materials

Gold NanoParticles (NPs) in colloidal solution (50 nm diameter; $4.5 \cdot 10^{10}$ particles/ml) were purchased from Ted Pella (Redding, CA). 4-aminothiophenol (4-ATP, Molecular Weight (MW) 125 Da), glutathione S-transferase (GST, MW 26 kDa), ethanolamine (ETA, MW 61 Da), mouse monoclonal anti-$p53_{wt}$ PAb 1620 antibody (anti-$p53_{wt}$, MW 150 kDa) and healthy human serum were purchased from Sigma-Aldrich (St. Louis, MO). Wild type p53 ($p53_{wt}$, MW 43 kDa) and the rabbit polyclonal anti-$p53_{R175H}$ antibody (anti-$p53_{R175H}$, MW 150 kDa) were purchased from Creative Biomart (Shirley, NY). Mutant $p53_{R175H}$ ($p53_{R175H}$, MW 43 kDa) was purchased from Genscript (Piscataway, NJ). Phosphate-buffered saline (PBS) solution 50 mM pH 7.2, hereafter buffer, was prepared by using reagents from Sigma Aldrich. p53 pan ELISA kit was purchased from Roche Diagnostics GmbH (Mannheim, Germany).

2.2. Probe assembly

4-ATP molecules and NPs (Fig. 1A) were linked through a covalent bond (S-Au) (Fig. 1B). The 4-ATP-NP reaction was optimized by varying the concentration of 4-ATP (between 10^{-2} and 10^{-9} M), the reaction temperature (25 °C, 30 °C, 40 °C) and the reaction time (3 h, 4 h, 24 h). The parameters were selected by following the shift of the absorption band of NPs, which is proportional to the number of bound 4-ATP molecules. Finally, 1 ml of the mother solution of NPs was mixed with 1 ml of 4-ATP ($4 \cdot 10^{-3}$ M in absolute ethanol) and the obtained solution was incubated at 25 °C for 3 h. To remove the excess of unbound 4-ATP and to promote the ethanol to Milli-Q water solvent exchange, the solution was dialyzed overnight by using a membrane with a MW cut-off of 100 kDa. The interaction between gold NPs and 4-ATP was followed by optical spectroscopy. Bare gold NP solution exhibited an absorption band centred at about 533 nm (Fig. 2, black line), which was attributed to the surface plasmon excitation of gold NPs [39]. Upon binding of NPs to 4-ATP, this band was broadened and upward shifted to 537 nm (Fig. 2, red line); with this indicating the formation of the 4-ATP/NP complex (Inset in Fig. 2) [31]. To covalently bind the antibody to 4-ATP/NP complex, a diazo coupling reaction was performed [40]. Briefly, such a reaction results into the formation of the diazonium compound ($-N^{+}\equiv N$), which is highly reactive, towards the histidine and tyrosine amino acids of proteins. Diazonium compound (Fig. 1C) was obtained by adding 500 µl of $NaNO_2$ (0.1 M, pH 3) to 500 µl of dialyzed 4-ATP/NP solution, very slowly and under constant stirring, for 15 min at 4 °C. Phenol was used to visually monitor the progress of the reaction. Excess of both nitrous and hydrochloric acid was removed by dialysis against Milli-Q ice water for 6 h and the resulting solution was stabilized at pH 7.2 by dialysing overnight against buffer at 4 °C [41,42]. 100 µl of anti-$p53_{wt}$ ($1.5 \cdot 10^{-6}$ M), or alternatively 100 µl of anti-$p53_{R175H}$ ($1.5 \cdot 10^{-6}$ M),

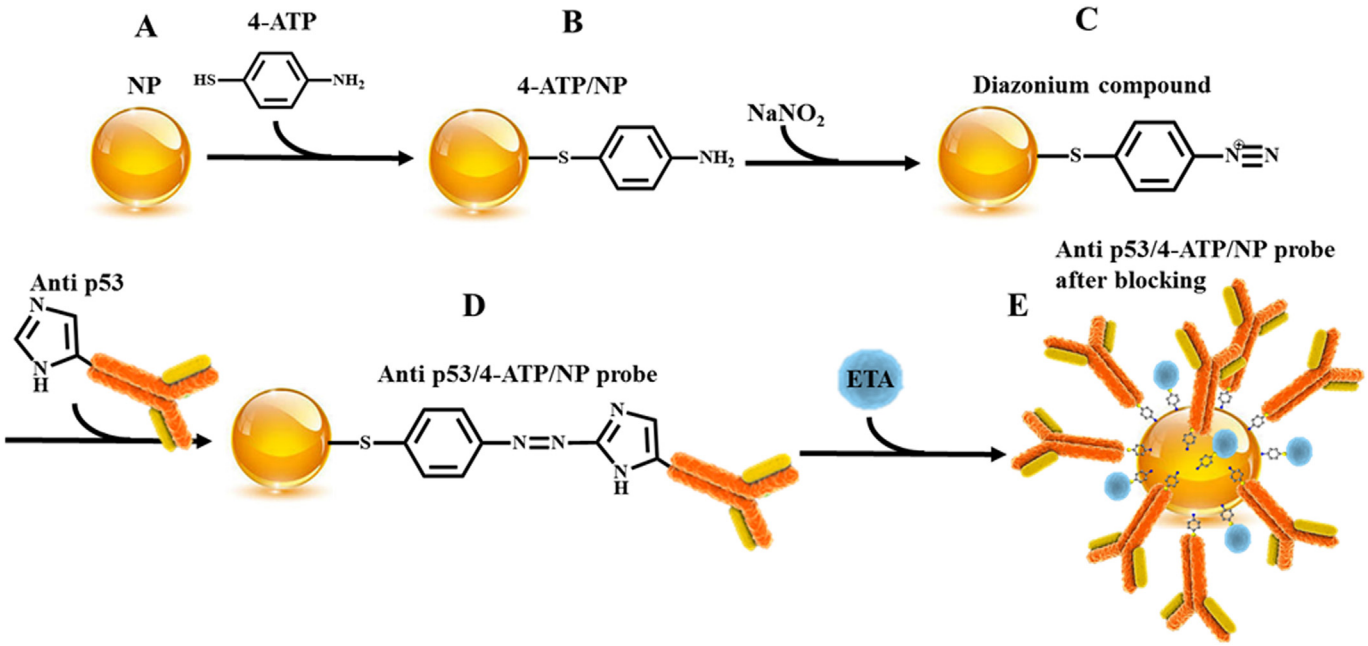

Fig. 1. Scheme of the chemical reaction steps leading to the functionalization of the NPs with anti-p53 molecules. (A) Bare NP; (B) reaction between NP and 4-ATP molecules, leading to the 4-ATP/NP complex; (C) formation of the diazonium compound; (D) reaction of 4-ATP/NP complex with anti-p53 to form the anti-p53/4-ATP/NP probe; and (E) blocking of unreacted sites of the anti-p53/4-ATP/NP probe with ETA. (not in scale).

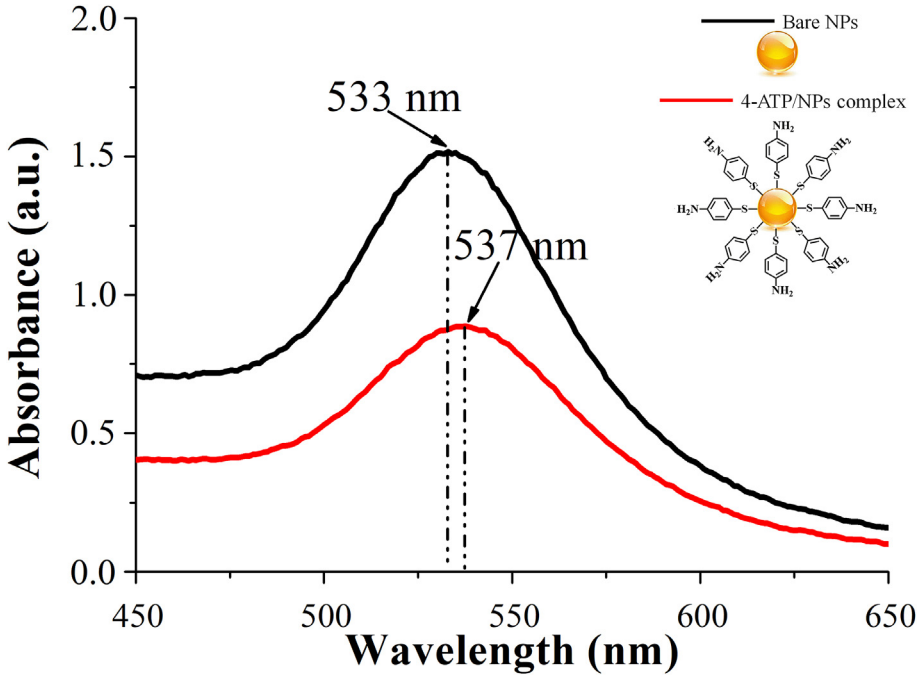

Fig. 2. Absorption spectrum of NPs before (black line) and after (red line) conjugation with 4-ATP. The maximum absorption peaks are marked. Inset: schematic representation of the two compounds. (For interpretation of the references to colour in this figure legend, the reader is referred to the Web version of this article.)

were then added to the diazonium compound solution (200 μl). The solution was kept under a gentle stirring at 4 °C for 2 h to obtain the anti-p53 probe (anti-p53/4-ATP/NP, Fig. 1D). In order to remove the excess of unbound anti-p53, the final solution was centrifuged at 8000 rpm for 5 min, the pellet was re-suspended in an equal volume of buffer and the overall procedure was repeated twice. To block unbound reactive sites on the NPs surface, 200 μl of the anti-p53/4-ATP/NP probe was incubated with 100 μl of 1 M ETA under a gentle stirring at 2 °C for 2 h (Fig. 1E). The solution was centrifuged at 8000 rpm for 5 min to remove the unbound ETA molecules and the pellet was re-suspended in 200 μl of buffer; such a procedure having been repeated twice [43].

2.3. Quantification of the antibody conjugated to NPs

Fig. 3 shows the fluorescence emission spectra of anti-p53$_{wt}$

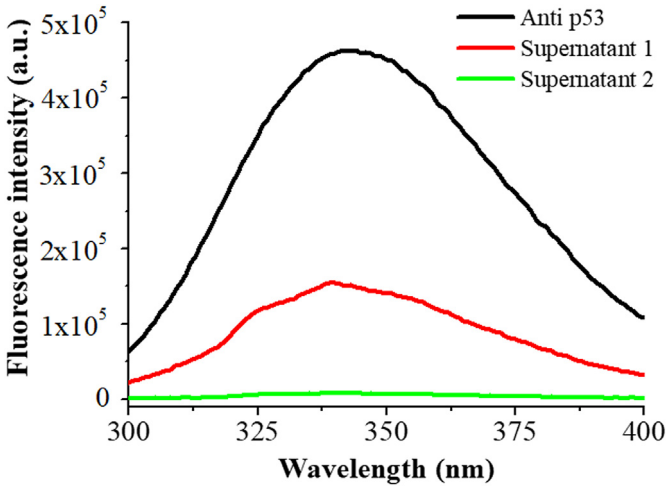

Fig. 3. Emission spectra of anti-$p53_{wt}$ in the reaction solution (black line) and of two supernatants (red and green lines), resulting from the centrifugation of the diazonium compound/anti-$p53_{wt}$ solution. Samples were excited at 280 nm and fluorescence emission was collected at 340 nm. (For interpretation of the references to colour in this figure legend, the reader is referred to the Web version of this article.)

(black line) upon 280 nm excitation, at the concentration used in the probe assembly, and of the supernatants obtained by two successive washing and centrifugation steps (red and green lines, respectively). The observed decrease of the fluorescence intensity for the two supernatants indicates that unbound anti-$p53_{wt}$ molecules were progressively removed. To evaluate the amount of the anti-$p53_{wt}$ conjugated to 4-ATP/NP ($C_{conjugated}$), the unbound anti-$p53_{wt}$ in the supernatants was estimated according to the expression [44]:

$$C_{conjugated} = C_0 - C_{unbound} = C_0\,(F_0 - F)/F_0 \quad (1)$$

where C_0 and F_0 are the concentration and fluorescence intensity of the initial sample and of anti-$p53_{wt}$, respectively; while $C_{unbound}$ and F are the concentration and the fluorescence intensity of the anti-$p53_{wt}$ in the supernatants, respectively. Accordingly, we estimated that about $2.5\bullet10^3$ molecules of anti-$p53_{wt}$, corresponding to a concentration of $1.9\bullet10^{-7}$ M of anti-$p53_{wt}$, were conjugated to a single NP. The same concentration was also estimated for the anti-$p53_{R175H}$ probe conjugated to a single NP.

2.4. Preparation of the capture substrate and of the probe

The functionalization of the substrates, able to capture the corresponding probe, was done by following the procedure sketched in Fig. 4A–E. First, glass substrates were cleaned by immersion in 100% acetone for 5 min, dried to N_2 and ultraviolet irradiated for 30 min to strongly increase the number of silanol groups on the surface (Fig. 4A). Successively, they were treated with 3-aminopropyltriethoxy-silane (APTES) dissolved in chloroform (6% solution) for 3 min to form a self-assembled monolayer. After rinsing three times with chloroform, and drying to N_2, they were reacted with 1% glutaraldehyde solution for 4 min at room temperature (Fig. 4B). Then, rinsing with Milli-Q water and drying to N_2 of the aldehyde-modified glass substrates was followed by incubation with 40 μl of $p53_{wt}$ or $p53_{R175H}$ proteins, at concentrations ranging from 10^{-10} M to 10^{-18} M in buffer, for 6 h at 4 °C (Fig. 4C); with the formation of the self-assembled protein monolayer through the solvent exposed amino groups being thus promoted. To block the unreacted sites (i.e. the sites of the functionalized substrate which had not reacted with p53 or its mutant), a two-step procedure was followed. First, the substrates were incubated with 40 μl of GST (10^{-10} M) overnight at 4 °C and then washed with buffer and N_2 dried (Fig. 4D). In this way, we found that the unreacted sites on the functionalized substrates could be more effectively blocked by GST, whose dimensions are comparable to those of p53, through a reaction involving its solvent exposed amino groups. To complete the blocking of the unreacted sites, the substrates were successively incubated with 40 μl of ETA (1 M) for 5 h at 4 °C, and subsequently washed with buffer and N_2 dried (Fig. 4E) [43,45]. Finally, these substrates, functionalized with the markers to be detected ($p53_{wt}$ or $p53_{R175H}$), were incubated with 10 μl of the probe (containing about 10^{-7} M of anti-p53), for 3 h at 4 °C, to promote the antigen-antibody biorecognition (Fig. 4F). The incubation times were in the 2–10 h range in the various steps and were optimized by monitoring the number of bright emitting sites (called hot spots [46–48]) showing the features of the anti-$p53_{wt}$/4-ATP/NP probe (see below). The substrates were then washed with buffer to remove the excess or unbound probe and N_2 dried.

Blank reference samples were prepared by incubating the glass slides, previously treated with APTES and glutaraldehyde, with GST and ETA, but without $p53_{wt}$ or $p53_{R175H}$. Experiments with serum were performed by incubating for 6 h at 4 °C the substrates, which had been previously functionalized with APTES and glutaraldehyde, with 40 μl of bare healthy human serum or of human serum spiked with $p53_{wt}$ or with $p53_{R175H}$, at concentrations ranging from 10^{-10} to 10^{-16} M [49]. Then, samples were treated with GST and ETA as above described. Finally, the substrates were washed with buffer and dried to N_2. The substrates were stored in a humid chamber at 4 °C and were found to be stable within two weeks and were used once. The same procedure for the incubation with the probe was followed for blank and serum samples.

2.5. Optical absorption, emission and SERS experiments

Absorption measurements on bare and functionalized NPs were carried out at room temperature using a two-beam photo spectrophotometer (V-550, Jasco) in the spectral region 450–650 nm with a 0.5 nm bandpass. Fluorescence measurements were carried out at room temperature using a Spectrofluorometer (FluoroMax^R-4 Spectrofluorometer, Horiba Scientific, Jobin Yvon). Samples were excited at 280 nm and fluorescence emission was collected from 295 to 400 nm by using 1 nm increments and an integration time of 0.5 s. A 3 nm bandpass was used in both the excitation and emission paths. Spectra were acquired in the signal to reference (S/R) mode to take into account for random lamp intensity fluctuations. Moreover, emission spectra were corrected for Raman contribution from the buffer. Raman and SERS experiments were performed by a Jobin-Yvon Super Labram confocal system (Horiba Scientific, Jobin Yvon), equipped by a liquid nitrogen-cooled CCD (EEV CCD10-11 back illuminated; pixel format: 1024 × 128 detector) and by a spectrograph with a 1800 g/mm grating. Spectra acquisition was performed according to back scattering geometry by using a notch filter to reject the elastic contribution. A diode-pumped solid-state laser emitting at 532 nm with a power of 10 mW (4.8 mW on the sample) was employed as the excitation source. Measurements were performed by using a 50× objective with a numerical aperture NA = 0.6; laser spot diameter reaching the sample being about 1 μm. The confocal diaphragm was 400 μm and the slit was 200 μm. A typical accumulation time of 100 s and a spectral resolution of 5 cm^{-1} were used. For each sample, a 3 × 3 mm^2 region of the functionalized substrate was manually scanned by the microscope objective to localize the hot spots; ten spectra were acquired for each sample. All spectra were vector normalized within the whole wavenumber range and processed by a concave rubber-band baseline correction in order to remove fluorescence background.

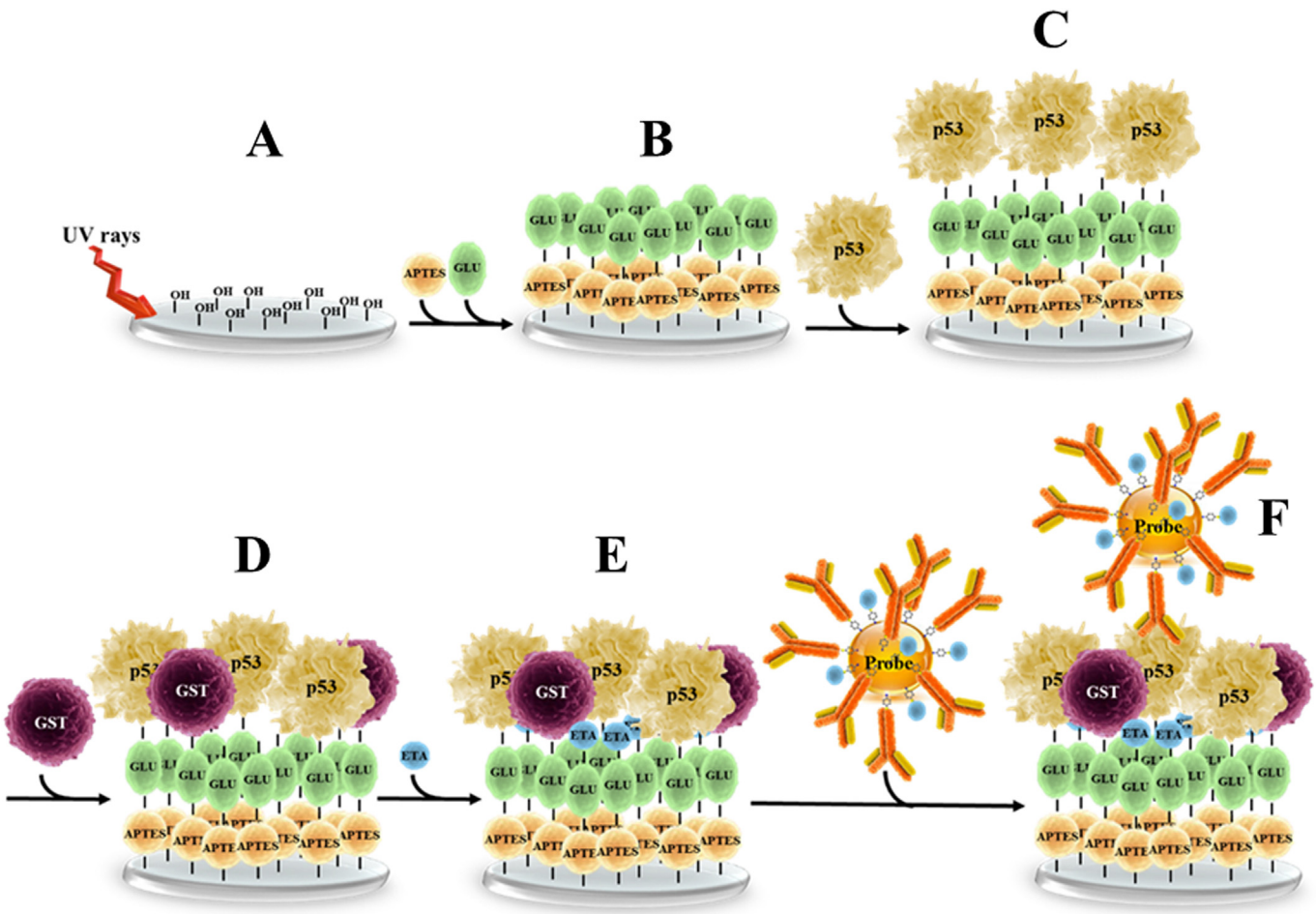

Fig. 4. Sketch of the main steps for the substrate functionalization. (A) UV ray treatment to increase the amount of silanol groups; (B) incubation with APTES and glutaraldehyde; (C) functionalization with p53; (D–E) blocking of unreacted sites with GST and ETA; and (F) incubation with the functionalized probe (not in scale).

The reproducibility of the results was assessed by repeating each experiment five times.

2.6. ELISA assay for p53 quantification

The photometric one-step-enzyme immunoassay (p53 pan ELISA kit, Roche Diagnostics) was used for the quantification of unknown samples of $p53_{R175H}$ (100 µl, diluted 1:5 in sample diluent). The assay is based on the quantitative "sandwich ELISA" principle in which a capture antibody is pre-coated onto a microtiter plate where the sample and the peroxidase-labelled detection antibody were incubated to form a stable immuno-complex. Subsequent to washing step, the peroxidase bound to the immuno-complex is developed by tetramethylbenzidine (TMB) as a substrate. The (A_{450nm}-A_{690nm}) of each sample was measured in duplicate by using a microplate spectrophotometer (Multiskan™ Go, ThermoScientific, Whaltam, MA), and its mean value was used for protein quantification by using a calibration curve obtained from human p53 standards, provided by the producer.

3. Results and discussion

3.1. Raman characterization of the probe

The SERS spectrum of the 4-ATP linker after conjugation with the NPs, is shown in Fig. 5A. Five main bands are detected in the 1000-1500 cm^{-1} region. In particular, bands at 1089 and 1176 cm^{-1} arise from C–S stretching and C–N bending modes of the benzene ring, respectively. The bands at 1423 and 1492 cm^{-1} can be associated to the C–C stretching vibrations, while the band at 1125 cm^{-1} was not assigned [18,50,51]. The disappearance of the band at 2555 cm^{-1}, due to the stretching vibration of free 4-ATP S–H group (Fig. 5A, Inset), witnesses the occurrence of 4-ATP conjugation to the NPs, *via* an S-Au covalent bond [41].

Fig. 5B shows the SERS spectrum of the antibody probe as obtained by conjugation of the 4-ATP/NP system with anti-p53 via the diazotization reaction involving the exposed histidine and/or tyrosine residues of the biomolecule. The obtained system will be named anti-$p53_{wt}$/4-ATP/NP probe in the following. We note in this probe the appearance of an additional strong Raman band centred at about 1328 cm^{-1} (highlighted in Fig. 5). The band is assigned to the stretching vibration modes of the diazo bond (N=N), which tightly keeps linked the antibody to the 4-ATP/NP and witnesses the occurrence of a covalent bond between 4-ATP/NP and the antibody [31,50]. Moreover, it constitutes a specific Raman fingerprint (or Raman marker), with well distinguishable vibrational features of the probe. The presence of this Raman signal, which results significantly enhanced by the plasmonic effect induced by the NPs, has been then exploited in our strategy for detection of p53 and its mutant with high sensitivity. A spectrum almost identical to that shown in Fig. 5B, was obtained by conjugating the 4-ATP/NP system with anti-$p53_{R175H}$ (not shown); with this constituting the

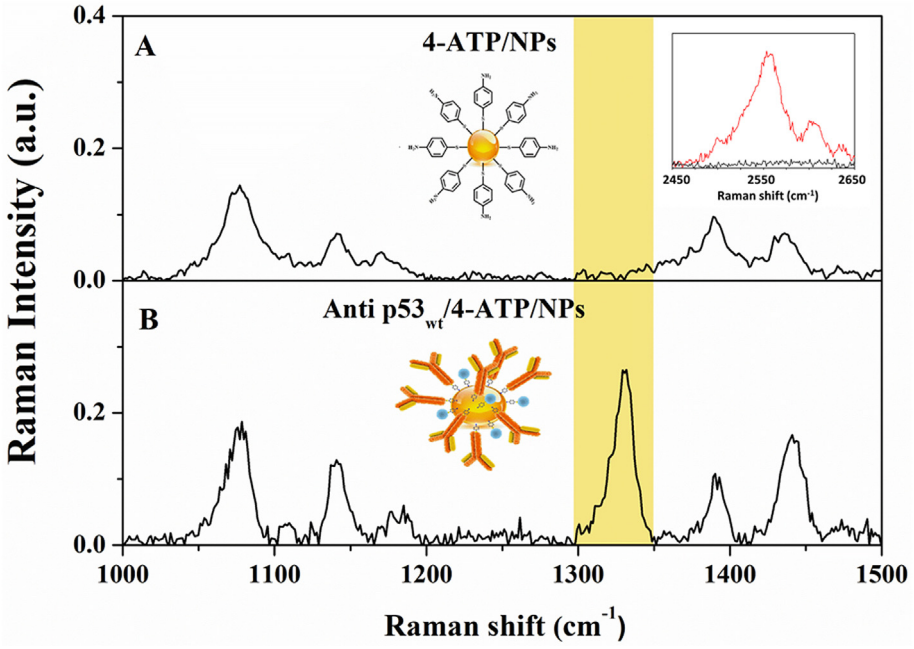

Fig. 5. (A) SERS spectrum of 4-ATP self-assembled on gold NPs. Inset: Raman signals in the range corresponding to the stretching mode of the SH group belonging to free 4-ATP (red line) and to 4-ATP bound to gold NPs (black line). (B) SERS spectrum of anti-$p53_{wt}$/4-ATP/NP probe. The yellow band highlights the Raman marker at 1328 cm^{-1}. In each box, a schematic representation of the corresponding probe assembly step is shown (not in scale). (For interpretation of the references to colour in this figure legend, the reader is referred to the Web version of this article.)

anti-$p53_{R175H}$/4-ATP/NP probe.

3.2. SERS detection of wild type and mutated p53 in buffer

The anti-$p53_{wt}$/4-ATP/NP probe was incubated with the capture substrates, which had been previously functionalized with $p53_{wt}$ at different concentrations (ranging from 10^{-10} to 10^{-18} M) (see Materials and Methods Section). Fig. 6A–C shows the SERS spectra corresponding to capture substrates functionalized with $p53_{wt}$ at 10^{-12}, 10^{-15} and 10^{-17} M. The observed characteristic Raman fingerprint at 1328 cm^{-1} (marked in yellow), corresponding to the stretching vibration of the diazo bond formed between the anti-$p53_{wt}$ and the 4-ATP/NP system, can be clearly detected down to 10 aM antigen concentration. The appearance of the Raman fingerprint witnesses the occurrence of a biorecognition process between $p53_{wt}$ and the anti-$p53_{wt}$/4-ATP/NP probe. At

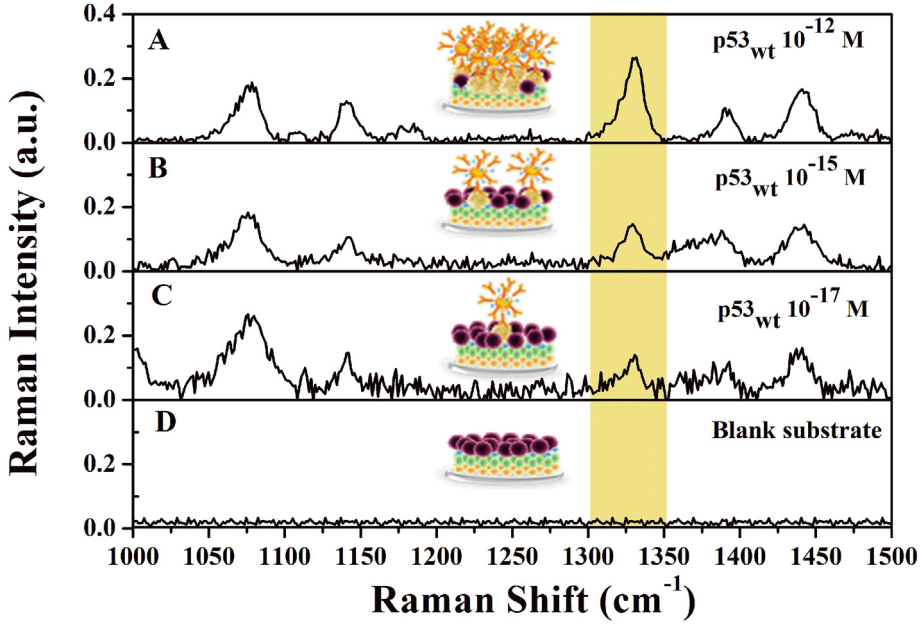

Fig. 6. SERS spectra of the samples obtained upon incubating the anti-$p53_{wt}$ probe on substrates functionalized with $p53_{wt}$ at different concentrations: 10^{-12} M (A), 10^{-15} M (B) and 10^{-17} M (C). Raman spectrum obtained upon incubating the anti-$p53_{wt}$/4-ATP/NP probe on the blank substrate; with this being used as negative control (D). The yellow band highlights the Raman marker at 1328 cm^{-1}. In each box, a schematic representation of the biorecognition event is shown (not in scale). (For interpretation of the references to colour in this figure legend, the reader is referred to the Web version of this article.)

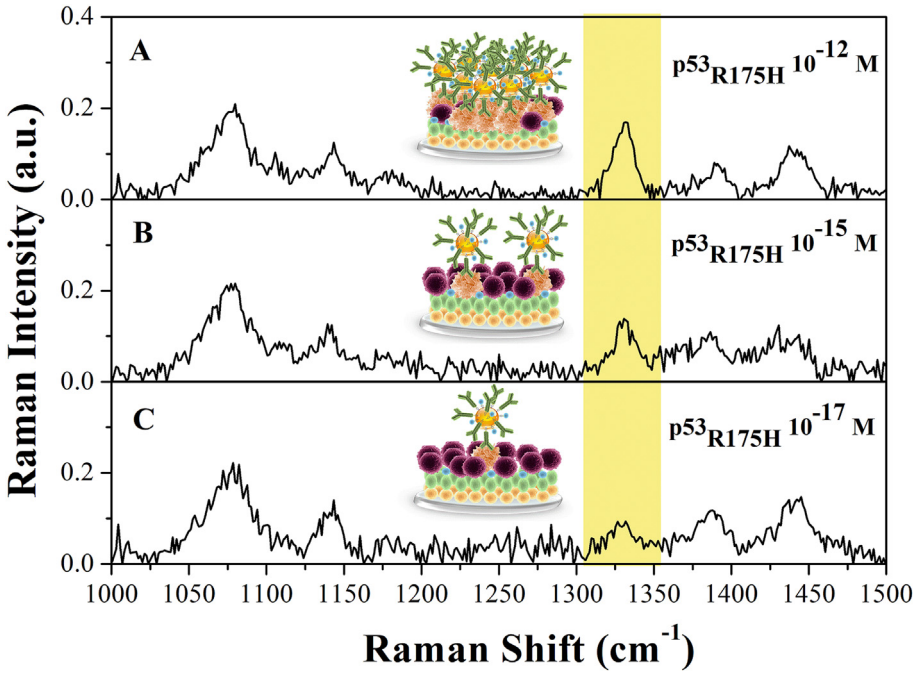

Fig. 7. SERS spectra of the samples obtained upon incubating the anti-p53$_{R175H}$ probe on substrates functionalized with p53$_{R175H}$ at different concentrations: (A) 10^{-12} M, (B) 10^{-15} M, and (C) 10^{-17} M. The yellow band highlights the Raman marker at 1328 cm^{-1}. In each box, a schematic representation of the biorecognition event is reported (not in scale). (For interpretation of the references to colour in this figure legend, the reader is referred to the Web version of this article.)

concentrations lower than 10^{-17} M, the signal of the Raman fingerprint becomes almost undetectable over the noise level (Fig. 6D).

Similar results were obtained when the anti-p53$_{R175H}$/4-ATP/NP probe was incubated with substrates functionalized with p53$_{R175H}$, in the 10^{-10} to 10^{-17} M concentration range. Again, the characteristic Raman fingerprint at 1328 cm^{-1} can be clearly observed for p53$_{R175H}$ concentrations down to 10^{-17} M (Fig. 7). We would like to emphasize that, to the best of our knowledge, such a low detection level was not reached till now for both p53$_{wt}$ and its mutant [10,14–17,19–21]. Such a high sensitivity exceeds that obtained in our previous works, also based on SERS detection [18,31], and in other literature reports [37,38]. The remarkable sensitivity of our approach stems also from a careful tailoring and standardization of both the substrate and the detection probe functionalization chemistry; indeed, we ascertained that the passivation of the substrate with both GST and ETA significantly lowered the non-specific signals also arising from the interaction of the probe with non-passivated capture substrate.

For control, we recorded the Raman spectra from samples obtained by incubating the anti-p53$_{wt}$/4-ATP/NP probe (or the anti-p53$_{R175H}$/4-ATP/NP probe) on the blank substrate (see Materials and Methods Section), and we found that they do not reveal any significant signal over the noise (Fig. 6D). In particular, the average intensity detected in the (1328 ± 10) cm^{-1} interval, as evaluated from ten spectra acquired at different sites of the same sample, does not exceed that of the noise as estimated in the (1800 ± 10) cm^{-1} spectral region, where no Raman signals are present (see also Table 1). Accordingly, we infer that the anti-p53$_{wt}$/4-ATP/NP probe (or the anti-p53$_{R175H}$/4-ATP/NP probe) does not undergo any detectable unspecific interaction with the blank substrate.

To check the reproducibility of our SERS data, we analyzed the intensity of the Raman fingerprint peak at 1328 cm^{-1} for five independently prepared samples containing either p53$_{wt}$ or p53$_{R175H}$ at 10^{-15} M concentration. Fig. 8A and B shows the average (over ten acquired spectra for each sample) and the corresponding standard deviation of the integrated area of the peak for the two sets of samples. We note that the five values of the integrated area are comparable, within the errors, for both sample sets.

The selectivity of our biosensor for possible cross-reactions between p53$_{wt}$ and p53$_{R175H}$, was checked by analysing the following samples: i) the anti-p53$_{wt}$/4-ATP/NP probe incubated with the substrate functionalized with p53$_{R175H}$ at 10^{-15} M; and ii) the anti-p53$_{R175H}$/4-ATP/NP probe incubated with the substrate functionalized with p53$_{wt}$ at 10^{-15} M. The Raman spectra from both samples did not reveal any characteristic Raman fingerprint at 1328 cm^{-1} over the noise level (see also Table 1). These results demonstrate that our method is able to well discriminate between the presence of the p53$_{R175H}$ mutant from that of the wild type isoform of p53. Such a selectivity level may deserve rewarding

Table 1
Detection of the signal at 1328 cm^{-1} (Raman fingerprint) over the noise for different combinations of substrates and probes.

Substrate Probe	Blank	p53$_{wt}$	p53$_{R175H}$	Blank Serum	p53$_{wt}$ Serum	p53$_{R175H}$ Serum	p53$_{wt}$ + p53$_{R175H}$ Serum
anti-p53$_{wt}$/4-ATP/NPs	NS	S	NS	NS	S	NS	S
anti-p53$_{R175H}$/4-ATP/NPs	NS	NS	S	NS	NS	S	S

NS=No Signal (as in Fig. 6D).
S=Signal.

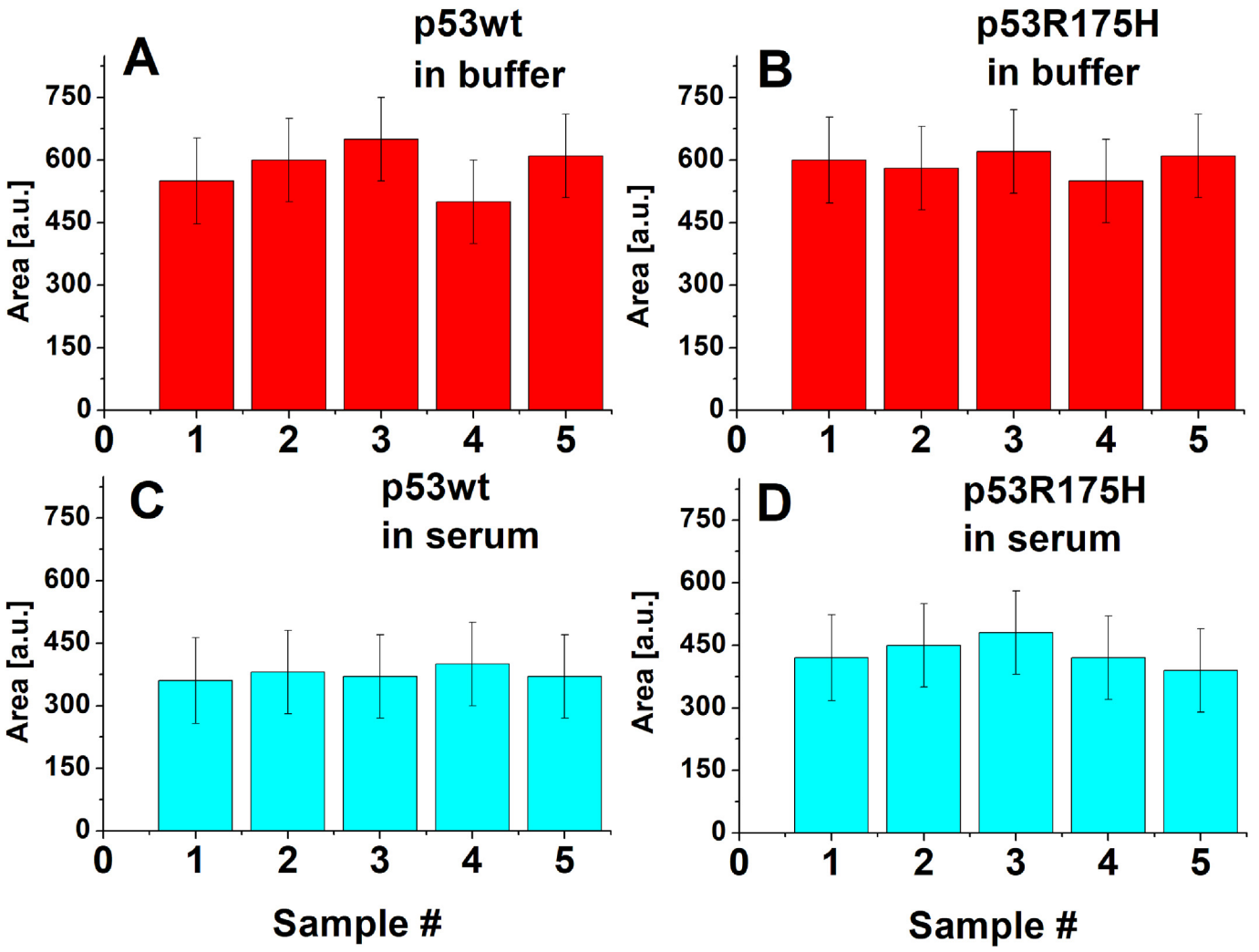

Fig. 8. Integrated area of the Raman peak at 1328 cm^{-1} for five different samples obtained by incubating the corresponding anti-p53 probe on substrates functionalized with: (A) $p53_{wt}$ in buffer; (B) $p53_{R175H}$ in buffer; (C) $p53_{wt}$ in human serum; (D) $p53_{R175H}$ in human serum. The average value and the corresponding standard deviation of the integrated area were obtained from ten spectra acquired at different regions of the sample.

applications in cancer diagnosis, especially when the simultaneous presence of both $p53_{wt}$ and $p53_{R175H}$ at low concentration occurs [12].

To reliably quantify the amount of p53 antigen samples with unknown concentration, we constructed a calibration plot (Fig. 9) of the average integrated area of the 1328 cm^{-1} peak as a function of the logarithm of both $p53_{wt}$ (squares) and $p53_{R175H}$ concentration (open circles). Notably, a very good linear relationship in the 10^{-10} and 10^{-17} M concentration range is observed in both cases. Accordingly, the data were fitted by the equation $Y = A + B^{*}X$, where Y is the averaged area intensity of the Raman marker peak and X is the logarithm of the corresponding p53 concentration (see continuous and dashed lines in Fig. 9). The fitting values A and B and the adjusted R^2 value, assessing the goodness of the fit, are shown in the same Figure. This linear calibration plot was then exploited to determine the concentration of two samples of $p53_{R175H}$ at unknown concentrations. In particular, upon measuring the average and the corresponding standard deviation of the 1328 cm^{-1} peak area from ten SERS spectra, the concentration and the related uncertainties of the unknown $p53_{R175H}$ samples were extracted from the calibration plot (see stars in Fig. 9 and Table 2, column 2). The reliability of these results was further tested by applying the p53 ELISA kit (Materials and Methods Section). We found that the concentrations as determined by ELISA (Table 2, column 3), are statistically consistent with those obtained by SERS experiments. Such an agreement validates our method with respect to its reliability in the quantification of p53.

Finally, we would like to note that the presented method could be easily implemented for the detection of other antigens on the substrate, by choosing the appropriate antibodies to be conjugated to the NP containing system, and also for the simultaneous detection of different biomarkers in multiplex assays [52].

3.3. SERS-based immunosensor for biorecognition of wild type and mutant p53 in human serum

With the aim at applying our SERS-based immunosensor to clinical purposes, we extended our method to the detection of both $p53_{wt}$ and $p53_{R175H}$ in human serum, in which the presence of these proteins could deserve a high interest in cancer diagnostics. For control, the substrate functionalized with bare healthy human serum was first analyzed. The Raman spectrum, shown in Fig. 10A, reveals the presence of two broad bands, at about 1050 and 1175 cm^{-1}, which are likely attributable to the lipids and phospholipids present in serum [53]. Successively, we analyzed the samples obtained by incubating the anti-$p53_{wt}$/4-ATP/NP (or anti-

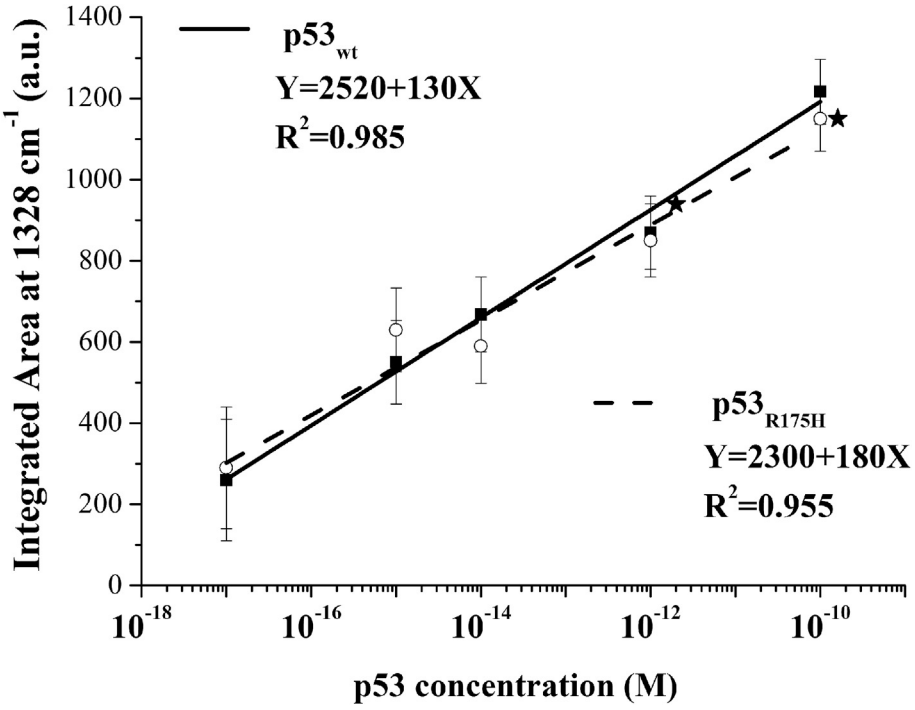

Fig. 9. Integrated area of the Raman peak at 1328 cm^{-1}, as a function of the logarithm of the $p53_{wt}$ concentration (squares) and of $p53_{R175H}$ (circles); the average value and the corresponding standard deviation of the integrated area were obtained from ten spectra acquired at different regions of the sample. The continuous line represents the fit of the $p53_{wt}$ data by the equation Y = A + BX with A=(2520 ± 110) and B=(133 ± 10); while the dashed line represents the fit of the $p53_{R175H}$ data by the equation Y = A + BX with A=(2300 ± 180) and B=(120 ± 14). The stars mark the integrated area for the unknown $p53_{R175H}$ samples.

Table 2
Concentration of two $p53_{R175H}$ samples as determined by SERS method (column 2) and, for control, by a commercial ELISA kit (column 3).

$p53_{R175H}$ Sample	SERS (pM)	ELISA (pM)
Unknown1	2.0 ± 0.6	1.8 ± 0.4
Unknown2	16.2 ± 0.8	15 ± 3

$p53_{R175H}$/4-ATP/NP) probe on the substrates previously functionalized with human serum spiked with $p53_{wt}$ (or $p53_{R175H}$) at a concentration ranging from 10^{-10} to 10^{-17} M. We found that the Raman fingerprint at 1328 cm^{-1} is clearly detectable for $p53_{wt}$ and $p53_{R175H}$ samples, down to 10^{-15} M; with representative SERS spectra being shown in Fig. 10B and C, respectively. At lower concentrations, the Raman fingerprint is no more detectable over the noise for both the $p53_{wt}$ and $p53_{R175H}$ samples. Accordingly, 10^{-15} M constitutes the detection limit of $p53_{wt}$ and $p53_{R175H}$ in human serum. For further control, we also analyzed the samples obtained by adding the anti-$p53_{wt}$/4-ATP/NP probe to the serum spiked with $p53_{wt}$ and $p53_{R175H}$; both of them at a concentration of 10^{-15} M. The SERS spectrum, shown in Fig. 10D, is almost equal to that obtained from the serum sample spiked only with $p53_{wt}$ (Fig. 10B); with this witnessing the absence of any interference in the detection of $p53_{wt}$ as due to the co-presence of $p53_{R175H}$, therefore confirming the ability of our method to discriminate between the p53 isoforms. Similar spectra were obtained also by using the anti-$p53_{R175H}$/4-ATP/NP probe on the serum sample spiked with both $p53_{wt}$ and $p53_{R175H}$ (see Table 1). Indeed, possible concentration-based interference between $p53_{wt}$ and its mutant could be evidenced from experiments conducted on samples at different ratios of the two p53 isoforms.

By following the same procedure applied for p53 in buffer, the reproducibility of the results for p53 in serum was assessed by comparing the average integrated area of the 1328 cm^{-1} peak from five samples (see Fig. 8C and D). Additionally, we note that the average area values (about 400 a. u.) are significantly lower with respect to those obtained in buffer at the same concentration (about 600 a. u.). Such a decrease can be ascribed to a reduction of the number of specific binding sites available in the functionalized substrates, likely due to a non-specific interaction involving the various biomolecules present in serum.

Finally, the possible cross-reaction between our probes (anti-$p53_{wt}$ and anti-$p53_{R175H}$) and the healthy human serum constituents was checked. The spectrum obtained by dropping the anti-$p53_{wt}$/4-ATP/NP probe on the bare healthy human serum-functionalized substrate, is practically the same of that shown in Fig. 10A, and it does not reveal any significant signal at 1328 cm^{-1} over the noise; with this being indicative that the probe was not captured by the substrate. A similar spectrum was also obtained by dropping the anti-$p53_{R175H}$/4-ATP/NP probe on the bare healthy human serum-functionalized substrate (see Table 1).

4. Conclusions

The proposed method was able to detect both $p53_{wt}$ and the oncogenic mutant $p53_{R175H}$, down to attomolar range in buffer and to femtomolar range in spiked human serum. Such an extremely high sensitivity was reached by coupling the huge SERS enhancement, arising from the peculiar Raman marker covalently linked to gold NPs with the high specificity of the antigen-antibody biorecognition process. The observed linear trend between the SERS intensity and the logarithm of the p53 concentration allowed us to derive a calibration plot whose accuracy was assessed by an ELISA kit. These properties, which are coupled with a high reproducibility and a remarkable selectivity in discriminating between $p53_{wt}$ and its $p53_{R175H}$ mutant, entitle our SERS-based immunosensing

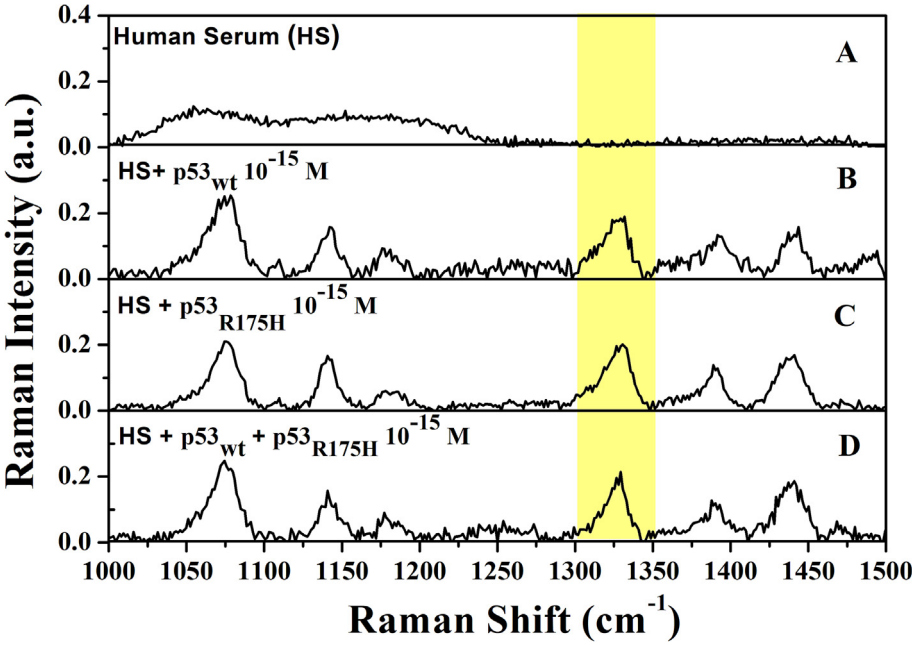

Fig. 10. SERS spectra of: (A) substrate functionalized with bare healthy human serum after incubation with the anti-$p53_{wt}$/4-ATP/NP probe; (B) substrate functionalized with human serum spiked with $p53_{wt}$ (10^{-15} M) after incubation with the anti-$p53_{wt}$/4-ATP/NP probe; (C) substrate functionalized with human serum spiked with $p53_{R175H}$ (10^{-15} M) after incubation with the anti-$p53_{R175H}$/4-ATP/NP probe; (D) substrate functionalized with human serum spiked with both $p53_{wt}$ (10^{-15} M) and $p53_{R175H}$ (10^{-15} M) after incubation with the anti-$p53_{wt}$/4-ATP/NP probe. The yellow band highlights the Raman marker at 1328 cm^{-1}. (For interpretation of the references to colour in this figure legend, the reader is referred to the Web version of this article.)

method to be used for clinical purposes. Collectively, the method deserves a high potentiality for easy, robust and reliable screening in extracellular fluid for early diagnosis of tumors, and also for prognosis and choice of a suitable therapy, targeting the specific p53 pathway.

The method could be easily implemented in a multiplex assay, in the perspective of designing lab-on-chip devices for applications in clinical diagnostics. The overall displayed features make the detection method highly versatile and easily exportable to the detection of other markers (for example in food control and environmental monitoring), upon linking to the gold NPs suitable antibodies able to capture the antigens of interest, immobilized on the substrate.

Acknowledgments

We thank the Italian Association for Cancer Research (AIRC) for financial support (Grant IG15866 to SC). We acknowledge a contribution to preliminary experiments from Drs. Michela Delfino and Sara Signorelli.

References

[1] B. Vogelstein, S. Sur, C. Prives, p53: the most frequently altered gene in human cancers, Nat. Educ 3 (2010) 6.
[2] J.P. Kruse, W. Gu, Modes of p53 regulation, Cell 137 (2009) 609–622, https://doi.org/10.1016/j.cell.2009.04.050.
[3] C. Kandoth, M.D. McLellan, F. Vandin, K. Ye, B. Niu, C. Lu, M. Xie, Q. Zhang, J.F. McMichael, M.A. Wyczalkowski, M.D.M. Leiserson, C.A. Miller, J.S. Welch, M.J. Walter, M.C. Wendl, T.J. Ley, R.K. Wilson, B.J. Raphael, L. Ding, Mutational landscape and significance across 12 major cancer types, Nature 502 (2013) 333–339, https://doi.org/10.1038/nature12634.
[4] M.J. Oh, J.H. Choi, Y.H. Lee, J.K. Lee, J.Y. Hur, Y.K. Park, K.W. Lee, S.Y. Chough, H.S. Saw, Mutant p53 protein in the serum of patients with cervical carcinoma: correlation with the level of serum epidermal growth factor receptor and prognostic significance, Canc. Lett. 203 (2004) 107–112.
[5] K.S. Shim, K.H. Kim, B.W. Park, S.Y. Lee, J.H. Choi, W.S. Han, E.B. Park, Increased serum levels of mutant p53 proteins in patients with colorectal cancer, J. Kor. Med. Sci. 13 (1998) 44–48, https://doi.org/10.3346/jkms.1998.13.1.44.
[6] A.M. Attallah, M.M. Abdel-Aziz, A.M. El-Sayed, A.A. Tabll, Detection of serum p53 protein in patients with different gastrointestinal cancers, Canc. Detect. Prev. 27 (2003) 127–131, https://doi.org/10.1016/S0361-090X(03)00024-2.
[7] A. Petitjean, E. Mathe, S. Kato, C. Ishioka, S.V. Tavtigian, P. Hainaut, M. Olivier, Impact of mutant p53 functional properties on TP53 mutation patterns and tumor phenotype: lessons from recent developments in the IARC TP53 database, Hum. Mutat. 28 (2007) 622–629, https://doi.org/10.1002/humu.20495.
[8] M. Wu, C. Mao, Q. Chen, X.-W. Cu, W.-S. Zhang, Serum p53 protein and anti-p53 antibodies are associated with increased cancer risk: a case–control study of 569 patients and 879 healthy controls, Mol. Biol. Rep. 37 (2010) 339–343, https://doi.org/10.1007/s11033-009-9744-7.
[9] G.A. Balogh, D.A. Mailo, M.M. Corte, P. Roncoroni, H. Nardi, E. Vincent, D. Martinez, M.E. Cafasso, A. Frizza, G. Ponce, E. Barutta, P. Lizarraga, G. Lizarraga, C. Monti, E. Paolillo, R. Vincent, R. Quatroquio, C. Grimi, H. Maturi, M. Aimale, C. Spinsanti, H. Montero, J. Santiago, L. Shulman, M. Rivadulla, M. Machiavelli, G. Salum, M.A. Cuevas, J. Picolini, A. Gentili, R. Gentili, J. Mordoh, Mutant p53 protein in serum could be used as a molecular marker in human breast cancer, Int. J. Oncol. 28 (2006) 995–1002.
[10] M.A. Levesque, M. D'Costa, E.P. Diamandis, P53 protein is absent from the serum of patients with lung cancer, Br. J. Canc. 74 (1996) 1434–1440.
[11] G.A. Balogh, D. Mailo, H. Nardi, M.M. Corte, E. Vincent, E. Barutta, G. Lizarraga, P. Lizarraga, H. Montero, R. Gentili, Serological levels of mutated p53 protein are highly detected at early stages in breast cancer patients, Exp. Ther. Med. 1 (2010) 357–361, https://doi.org/10.3892/etm.
[12] R.F. Service, Rescuing the guardian of the genome, Science 354 (2016) 26–28.
[13] A.I. Robles, J. Jen, C.C. Harris, Clinical outcomes of TP53 mutations in cancers, Cold Spring Harb Perspect Med 6 (2016), https://doi.org/10.1101/cshperspect.a026294.
[14] E. Paleček, H. Černocká, V. Ostatná, L. Navrátilová, M. Brázdová, Electrochemical sensing of tumor suppressor protein p53-deoxyribonucleic acid complex stability at an electrified interface, Anal. Chim. Acta 828 (2014) 1–8, https://doi.org/10.1016/j.aca.2014.03.029.
[15] H. Afsharan, F. Navaeipour, B. Khalilzadeh, H. Tajalli, M. Mollabashi, M.J. Ahar, M.R. Rashidi, Highly sensitive electrochemiluminescence detection of p53 protein using functionalized Ru-silica nanoporous@gold nanocomposite, Biosens. Bioelectron. 80 (2016) 146–153, https://doi.org/10.1016/j.bios.2016.01.030.
[16] W. Zhou, Y. Ma, H. Yang, Y. Ding, X. Luo, A label-free biosensor based on silver nanoparticles array for clinical detection of serum p53 in head and neck squamous cell carcinoma, Int. J. Nanomed. 6 (2011) 381–386, https://doi.org/10.2147/IJN.S13249.
[17] S.H. Han, S.K. Kim, K. Park, S.Y. Yi, H.J. Park, H.K. Lyu, M. Kim, B.H. Chung, Detection of mutant p53 using field-effect transistor biosensor, Anal. Chim. Acta 665 (2010) 79–83, https://doi.org/10.1016/j.aca.2010.03.006.
[18] F. Domenici, A.R. Bizzarri, S. Cannistraro, SERS-based nanobiosensing for ultrasensitive detection of the p53 tumor suppressor, Int. J. Nanomed. 6 (2011)

2033–2042, https://doi.org/10.2147/IJN.S23845.
[19] P. Owens, N. Phillipson, J. Perumal, G.M. O'Connor, M. Olivo, Sensing of p53 and EGFR biomarkers using high efficiency SERS substrates, Biosensors 5 (2015) 664–677, https://doi.org/10.3390/bios5040664.
[20] X. Jiang, L. Zhou, J. Cheng, H. Zhang, H. Wang, Z. Chen, F. Shi, C. Zhu, A novel method for the sensitive detection of mutant proteins using a covalent-bonding tube-based proximity ligation assay, Anal. Chim. Acta 841 (2014) 17–23, https://doi.org/10.1016/j.aca.2014.06.044.
[21] Y. Zhao, D. Du, Y. Lin, Glucose encapsulating liposome for signal amplification for quantitative detection of biomarkers with glucometer readout, Biosens. Bioelectron. 72 (2015) 348–354, https://doi.org/10.1016/j.bios.2015.05.028.
[22] M. Mattioni, P. Chinzari, S. Soddu, L. Strigari, V. Cilenti, E. Mastropasqua, Serum p53 antibody detection in patients with impaired lung function, BMC Canc. 13 (2013) 62, https://doi.org/10.1186/1471-2407-13-62.
[23] J.F. Rusling, C.V. Kumar, J.S. Gutkind, V. Patel, Measurement of biomarker proteins for point-of-care early detection and monitoring of cancer, Analyst 135 (2010) 2496–2511, https://doi.org/10.1016/j.pestbp.2011.02.012.Investigations.
[24] P. Csermely, K.S. Sandhu, E. Hazai, Z. Hoksza, H.J.M. Kiss, D. V Veres, F. Piazza, R. Nussinov, Disordered proteins and network disorder in network descriptions of protein structure, dynamics and function. Hypotheses and a comprehensive review, Curr. Protein Pept. Sci. (2011) 1–27, https://doi.org/10.2174/138920312799277992.
[25] S. Signorelli, S. Cannistraro, A.R. Bizzarri, Structural characterization of the intrinsically disordered protein p53 using Raman spectroscopy, Appl. Spectrosc. 71 (2017) 823–832, https://doi.org/10.1177/0003702816651891.
[26] A. Campion, P. Kambhampati, M.J. Weaver, M.J. Natan, V.M. Shalaev, J.S. Suh, R. Botet, Surface-enhanced Raman scattering, Chem. Soc. Rev. 27 (1998) 241, https://doi.org/10.1039/a827241z.
[27] S.D. Hudson, G. Chumanov, Bioanalytical applications of SERS (surface-enhanced Raman spectroscopy), Anal. Bioanal. Chem. 394 (2009) 679–686, https://doi.org/10.1007/s00216-009-2756-2.
[28] S. Boca, C. Farcau, M. Baia, S. Astilean, Metanephrine neuroendocrine tumor marker detection by SERS using Au nanoparticle/Au film sandwich architecture, Biomed. Microdevices 18 (2016) 12, https://doi.org/10.1007/s10544-016-0037-3.
[29] S. Harmsen, M.A. Bedics, M.A. Wall, R. Huang, M.R. Detty, M.F. Kircher, Rational design of a chalcogenopyrylium-based surface-enhanced resonance Raman scattering nanoprobe with attomolar sensitivity, Nat. Commun. 6 (2015) 6570, https://doi.org/10.1038/ncomms7570.
[30] L. Xu, W. Yan, W. Ma, H. Kuang, X. Wu, L. Liu, Y. Zhao, L. Wang, C. Xu, SERS encoded silver pyramids for attomolar detection of multiplexed disease biomarkers, Adv. Mater. 27 (2015) 1706–1711, https://doi.org/10.1002/adma.201402244.
[31] F. Domenici, A.R. Bizzarri, S. Cannistraro, Surface-enhanced Raman scattering detection of wild-type and mutant p53 proteins at very low concentration in human serum, Anal. Biochem. 421 (2012) 9–15, https://doi.org/10.1016/j.ab.2011.10.010.
[32] E. Gabellieri, M. Bucciantini, M. Stefani, P. Cioni, Does azurin bind to the transactivation domain of p53? A Trp phosphorescence study, Biophys. Chem. 159 (2011) 287–293, https://doi.org/10.1016/j.bpc.2011.07.008.
[33] D. Apiyo, P. Wittung-Stafshede, Unique complex between bacterial azurin and tumor-suppressor protein p53, Biochem. Biophys. Res. Commun. 332 (2005) 965–968, https://doi.org/10.1016/j.bbrc.2005.05.038.
[34] A.R. Bizzarri, S. Cannistraro, Atomic Force Spectroscopy in biological complex formation: strategies and perspectives, J. Phys. Chem. B 113 (2009) 16449–16464, https://doi.org/10.1021/jp902421r.
[35] W.D. Hazelton, E.G. Luebeck, Biomarker-based early cancer detection: is it achievable? Sci. Transl. Med. 3 (2011) https://doi.org/10.1126/scitranslmed.3003272, 109fs9.
[36] M. Guo, J. Dong, W. Xie, L. Tao, W. Lu, Y. Wang, W. Qian, SERS tags-based novel monodispersed hollow gold nanospheres for highly sensitive immunoassay of CEA, J. Mater. Sci. 50 (2015) 3329–3336, https://doi.org/10.1007/s10853-015-8825-3.
[37] Y. Wang, L.-J. Tang, J.-H. Jiang, Surface-Enhanced Raman Spectroscopy-based, homogeneous, multiplexed immunoassay with antibody-fragments-decorated gold nanoparticles, Anal. Chem. 85 (2013) 9213–9220, https://doi.org/10.1021/ac4019439.
[38] J. Smolsky, S. Kaur, C. Hayashi, S.K. Batra, A.V. Krasnoslobodtsev, Surface-enhanced Raman scattering-based immunoassay technologies for detection of disease biomarkers, Biosensors 7 (2017), https://doi.org/10.3390/bios7010007.
[39] M.A.K. Abdelhalim, M.M. Mady, M.M. Ghannam, Physical properties of different gold nanoparticles: ultraviolet-visible and fluorescence measurements, J. Nanomed. Nanotechnol. 3 (2012) 178–194, https://doi.org/10.4172/2157-7439.1000133.
[40] H. Higgins, D. Fraser, The reaction of amino acids and proteins with diazonium compounds. I. A Spectrophotometric study of azo-derivatives of histidine and tyrosine, Aust. J. Chem. 5 (1952) 736–753, https://doi.org/10.1071/CH9520736.
[41] A.R. Bizzarri, S. Cannistraro, SERS detection of thrombin by protein recognition using functionalized gold nanoparticle, Nanomedicine 3 (2007) 306–310, https://doi.org/10.1016/j.nano.2007.09.005.
[42] J.H. Phillips, S.A. Robrish, C. Bates, High efficiency coupling of diazonium ions to proteins and amino acids, J. Biol. Chem. 240 (1965) 699–704.
[43] C.C. Lin, Y.M. Yang, Y.F. Chen, T.S. Yang, H.C. Chang, A new protein A assay based on Raman reporter labeled immunogold nanoparticles, Biosens. Bioelectron. 24 (2008) 178–183, https://doi.org/10.1016/j.bios.2008.03.035.
[44] D. Sotnikov, A. Zherdev, B. Dzantiev, Development and application of a label-free fluorescence method for determining the composition of gold nanoparticle–protein conjugates, Int. J. Mol. Sci. 16 (2014) 907–923, https://doi.org/10.3390/ijms16010907.
[45] Y.S. Sun, X. Zhu, Characterization of bovine serum albumin blocking efficiency on epoxy-functionalized substrates for microarray applications, J. Lab. Autom. 21 (2016) 625–631, https://doi.org/10.1177/2211068215586977.
[46] K. Kneipp, Y. Wang, H. Kneipp, L.T. Perelman, I. Itzkan, Single molecule detection using surface-enhanced Raman scattering (SERS), Phys. Rev. Lett. 78 (1997) 1667–1670, https://doi.org/10.1103/PhysRevLett.78.1667.
[47] A.R. Bizzarri, S. Cannistraro, Surface-Enhanced Resonance Raman spectroscopy signals from single myoglobin molecules, Appl. Spectrosc. 56 (2002) 1531–1537.
[48] A.R. Bizzarri, S. Cannistraro, Statistical analysis of intensity fluctuations in single molecule SERS spectra, Phys. Chem. Chem. Phys. 9 (2007) 5315–5319, https://doi.org/10.1039/b706008d.
[49] I. Moscetti, E. Teveroni, F. Moretti, A.R. Bizzarri, S. Cannistraro, MDM2-MDM4 molecular interaction investigated by atomic force spectroscopy and surface plasmon resonance, Int. J. Nanomed. 11 (2016) 4221–4229, https://doi.org/10.2147/IJN.S114705.
[50] L.S. Jiao, L. Niu, J. Shen, T. You, S. Dong, A. Ivaska, Simple azo derivatization on 4-aminothiophenol/Au monolayer, Electrochem. Commun. 7 (2005) 219–222, https://doi.org/10.1016/j.elecom.2004.12.014.
[51] M.J. Baker, S.R. Hussain, L. Lovergne, V. Untereiner, C. Hughes, R.A. Lukaszewski, G. Thiéfin, G.D. Sockalingum, Developing and understanding biofluid vibrational spectroscopy: a critical review, Chem. Soc. Rev. 45 (2016) 1803–1818, https://doi.org/10.1039/C5CS00585J.
[52] L. Wu, Z. Wang, S. Zong, H. Chen, C. Wang, S. Xu, Y. Cui, Simultaneous evaluation of p53 and p21 expression level for early cancer diagnosis using SERS technique, Analyst 138 (2013) 3450–3456, https://doi.org/10.1039/c3an00181d.
[53] J. Saade, M. Tadeu, T. Pacheco, M.R. Rodrigues, Identification of hepatitis C in human blood serum by near-infrared Raman spectroscopy, Spectroscopy 22 (2008) 387–395, https://doi.org/10.3233/SPE-2008-0344.